SUPPLEMENTARY INFORMATION

Clustering of IP_3 receptors by IP_3 retunes their regulation by IP_3 and Ca^{2+}

Taufiq-Ur-Rahman[1], Alexander Skupin[2], Martin Falcke[2,3] & Colin W. Taylor[1]

[1]Department of Pharmacology, Tennis Court Road, Cambridge, CB2 1PD, UK.
[2]Mathematical Cell Physiology, Max Delbrück Centre for Molecular Medicine, Robert Rössle Str. 10, 13092 Berlin, Germany. [3]Helmoholtz Centre Berlin for Materials and Energy, Glienicker Str. 100, 14109 Berlin, Germany.

Abbreviations

γ	Single channel conductance.
i	Single channel current.
N, n	Total number of IP_3R within a patch (N), number of IP_3R under consideration (n); $N \geq n$.
NP_o	Experimentally determined collective activity of all IP_3R within a patch (see equation 2).
P_o	Single channel open probability, whether measured directly from a single channel patch (where $P_o = P_{lone}$) or calculated from NP_o for a multi-channel patch assuming that each channel behaves independently ($P_o = NP_o/N$).
P_{lone}	P_o determined from a patch containing a single IP_3R.
τ_o, (τ_c)	Apparent mean open (closed) time of a single IP_3R.
$\tau_{o,N}$	Apparent mean duration of openings in which all N IP_3R are simultaneously open.
τ_{ib}	Mean duration of events when all channels are closed in a patch containing N IP_3R (i.e. inter-burst interval).

Materials and Methods

Culture of DT40 cells expressing rat IP_3R3 or IP_3R1

DT40 cells lacking genes for all three IP_3R subtypes (DT40-KO cells)[27] and the same cells stably transfected with rat IP_3R3 (DT40-IP_3R3 cells) or rat IP_3R1 (DT40-IP_3R1 cells)[10] were maintained in RPMI 1640 medium supplemented with 10% foetal bovine serum, 1% heat-inactivated chicken serum, 2 mM L-glutamine and 10 mM 2-mercaptoethanol at 37°C in a humidified atmosphere containing 5% CO_2. Cells were passaged (at ~ 2 x 10^6 cells/ml) every 2-3 days. Expression of IP_3R3 was quantified by immunoblotting with an antiserum specific for IP_3R3 (Transduction Laboratories)[10].

IP_3-evoked Ca^{2+} release from intracellular stores

Ca^{2+} uptake and release from the intracellular stores of populations of saponin-permeabilized DT40-IP_3R3 cells was measured using a low-affinity Ca^{2+} indicator (Mag-fluo-4) trapped within the ER[28].

Single channel recording from nuclear patches

Nuclei were isolated by lysis of DT40 cells[25] and allowed to adhere in bathing solution (BS, 1 ml) to a petri dish coated with poly-D-ornithine (Sigma). BS had the following composition: 140 mM KCl, 10 mM Hepes, 100 μM BAPTA, 51 μM $CaCl_2$ (free $[Ca^{2+}]$ =

211 ± 9 nM), pH 7.1. Free Ca^{2+} concentrations were computed using WinMaxC (http://www.stanford.edu/~cpatton/maxc.html) and confirmed using fluorescent Ca^{2+} indicators[10] and Ca^{2+}-sensitive electrodes. The measured values are shown in the table below. Pipettes were pulled from thick-walled borosilicate glass capillaries (GC150F, Harvard Instruments) and fire-polished. The pipette tip resistance was 10-15 MΩ when filled with pipette solution (PS: 140 mM KCl, 10 mM Hepes, 500 μM BAPTA, 258 μM $CaCl_2$ (free $[Ca^{2+}]$ = 229 ± 24 nM), 5 mM Na_2ATP, pH 7.1). Variations in the composition of PS including addition of IP_3 (American Radiolabeled Chemicals) are described in the text. Recordings were at 22°C with patches excised from the on-nucleus configuration. To prevent formation of vesicles, excised patches were sometimes exposed to air for 1-5 s. Seals with resistances >5 GΩ were routinely obtained. Currents were amplified using an Axopatch 200B amplifier, filtered at 1 kHz (-3dB) and digitized at 10 kHz with a Digidata 1322A interface and pClamp 9.2 software (Axon Instruments). Unless otherwise stated, all recordings were at +40 mV. Open channel noise precluded use of lesser filtering to improve the temporal resolution of our recordings.

	Nominal free $[Ca^{2+}]$, nM	Measured free $[Ca^{2+}]$, nM
BS	200	211 ± 9 (n = 4)[a]
PS	200	229 ± 24 (n = 4)[a]
PS	1000	1498 ± 93 (n = 4)[a]
PS	1000	1450 ± 210 (n = 4)[b]

[a]Determined with fluo 3; [b]determined with a Ca^{2+}-selective electrode.

Flash photolysis of caged IP_3

For flash photolysis experiments, pipettes were prepared from thin-walled, non-filamented borosilicate glass capillaries (Harvard Instruments). Pipettes had resistances of 15-20 MΩ when filled with PS. PS contained 100 μM D-*myo*-inositol 1,4,5-trisphosphate, (4,5)-1-(2-nitrophenyl) ethyl ester ("caged IP_3", Calbiochem). After recording for 30-60 s, IP_3 was released into PS by photolysis of caged IP_3 using a single high-intensity flash (1 ms) from a Xe-flash lamp (XF-10, Hi-Tech Scientific; 240 J with the capacitor charged to 385 V) passed through a filter (300-350 nM)[29,30].

Analysis of patch-clamp records

Currents were idealized using the segmental k-means (SKM) hidden-Markov algorithm of the QuB suite (www.qub.buffalo.edu) at full bandwidth (1 kHz) initially using a simple two state scheme (C ⇆ O)[31].

For both single and multi-IP_3R patches, the probability ($P_{o,n}$) of channels simultaneously opening to the n^{th} current level, was calculated from the ratio of the area of the n^{th} current level ($A_{o,,n}$) to the total area (A_{total}) of the amplitude histogram[32]:

$$P_{o,n} = \frac{A_{o,n}}{A_{total}} = \frac{A_{o,n}}{A_{closed} + \sum_{n=1}^{n=N} A_{o,n}} \qquad (\mathbf{1})$$

NP_o was calculated from[33,34]:

$$NP_o = \frac{\sum_{n=1}^{N}(n.t_n)}{T} \qquad (2)$$

where: t_n is the total time for which n IP_3R are simultaneously open, and T is the duration of the recording.

For single channel records, dwell time analysis used the MIL module of QuB with retrospective imposition of a dead time of 200 μs for approximate correction of missed events[31]. Dwell time distributions were analysed according to[35,36]. Mean dwell times are presented as 'apparent' values because of our inability to resolve events briefer than the dead time of the system.

The best gating scheme (based on the log-likelihood ratio) comprised two closed (C) states connected linearly to an open (O) state, with either of the following topologies: $C_1 \leftrightarrow O \leftrightarrow C_2$ or $C_2 \leftrightarrow C_1 \leftrightarrow O$. Both topologies are equally compatible with the observed bursting behaviour of IP_3R stimulated with a maximal concentration of IP_3: each returns almost identical values for the dwell-time constants and their amplitudes (Rahman and Taylor, unpublished observation)[37]. Our present analyses and simulations focus on IP_3R stimulated with saturating concentrations of IP_3 and on changes in P_o and τ_o (which are the same for both topologies). For simplicity we therefore use the $C_2 \leftrightarrow C_1 \leftrightarrow O$ scheme (Fig. 1d). This scheme predicts accurately the behaviour of both lone and clustered IP_3R (Supplementary Fig. 6, Supplementary Table 4).

For determination of τ_o from flash photolysis experiments, single channel open events within each 0.5 s time bin were separately idealized and the open times from all recordings were pooled, exported to ClampFit and fitted empirically using the method of maximum likelihood[38].

Reliable counting of IP_3R within nuclear patches

The number of active IP_3R (N) within a nuclear patch can be confidently ($p < 0.01$) equated to the maximum number of multiples of the unitary current level observed throughout a recording lasting longer than $5(\sigma_{N+1})$ (Ref. 12), where:

$$\sigma_N = \left[\frac{\tau_o}{N(P_o)^N}\right]\exp\left(\frac{N \times t_D}{\tau_o}\right) \qquad (3)$$

where, σ_N = the mean interval between successive simultaneous openings of all N IP_3R, t_D = minimum duration of an open event detectable after filtering (= 200 μs). Under typical recording conditions with 200 nM cytosolic free $[Ca^{2+}]$ and 10 μM IP_3, IP_3R within a cluster have $P_o = 0.25$, and $\tau_o = 5.6$ ms. A recording of >2.06 s is therefore sufficient confidently to identify 3 IP_3R within such a patch. The largest number of IP_3R/patch reported herein (8, after pre-treatment of nuclei with IP_3, Fig. 3a) requires a recording of >1125 s. All recordings lasted >30 s, those addressing the effects of pre-treatment with IP_3 (Fig. 3) lasted >10 min, and those assessing the effects of lower concentrations of IP_3 typically lasted 5-15 min.

Predicting P_o assuming independent IP_3R in multi-IP_3R patches
If a patch contains N identical and independent IP_3R, each with a probability P_o of being open, the probability of n channels being simultaneously open is given by the binomial distribution[39]:

$$P_{o,n} = \frac{N!}{n!(N-n)!} P_o^{n} (1-P_o)^{N-n} \qquad (4)$$

The predicted P_o of a single IP_3R in a patch containing several (N) IP_3R was calculated from the probability of all N channels being simultaneously open ($P_{o,N}$):

$$P_o = \sqrt[N]{P_{o,N}} \qquad (5)$$

For convenience, the equivalent analysis of P_o for multi-IP_3R patches exposed to high-Ca^{2+} (Fig. 4) used NP_o/N to calculate P_o and so to assess whether IP_3R opened independently. This is justified because with 1 μM Ca^{2+}, NP_o of multi-IP_3R patches matches that expected from the sum of the behaviour of lone IP_3R (Fig. 4c).

Comparisons of the kinetic behaviour of single- and multi-IP_3R patches
For multi-IP_3R patches containing N IP_3R, τ_o and τ_c2 were estimated as described[40,41]:

$$\tau_o = N.\tau_{o,N} \qquad (6)$$
$$\tau_c2 = N.\tau_{ib} \qquad (7)$$

For a patch with N IP_3R, τ_c2 obtained from equation 7 is the average duration of gaps between the opening bursts of each individual IP_3R.

Comparison of the number of transitions between IP_3R states for lone and paired IP_3R exposed to 1 μM Ca^{2+}
For IP_3R stimulated with 10 μM IP_3 and 1 μM Ca^{2+}, observed numbers of transitions to each of the 3 states in patches with 2 IP_3R (C, O1 and O2) were compared with the predicted numbers assuming that each IP_3R behaved independently[26]. Briefly, all transitions (18076 ± 3808 transitions/recording, n = 6) during a 2-min recording were counted. P_o derived from patches containing only a single IP_3R stimulated under identical conditions was used to predict the expected number of transitions to each state. The results are shown in Fig. 4g and Supplementary Fig 9.

Data analysis
Prism 4 (GraphPad Software Inc) was used for statistical analyses, with $p < 0.05$ denoting significance. Student's t-test and one-way ANOVA were used as appropriate to determine significance, and χ^2 test for comparing observed and predicted distributions. Concentration-response relationships were fitted by a Hill equation using a non-linear iterative, least-squares fitting (unweighted) procedure (GraphPad Prism 4):

$$P_o = P_{o(max)}/(1+EC_{50}/[IP_3]^n) \qquad (8)$$

where,
EC_{50}, half-maximally effective concentration of IP_3.
n, Hill coefficient.

Supplementary Discussion

Spacing of IP_3R before and after clustering

Our experimental analysis shows that the decreased P_o of clustered IP_3R cannot result from Ca^{2+} passing through IP_3R regulating the activities of neighbouring IP_3R. With identical free [Ca^{2+}] in BS and PS (200 nM), any Ca^{2+} flux at the holding potential of +40 mV used for most analyses would be small, away from the cytosolic surface of the IP_3R, and rapidly buffered by BAPTA. Furthermore, in two experiments with patches containing 3 IP_3R and performed at a holding potential of -40 mV, when any Ca^{2+} flux would be in the opposite direction (i.e. towards the cytosolic surface of the IP_3R), the effects of clustering were indistinguishable from those observed at positive holding potentials. Under these conditions, the three IP_3R were independently gated, but with a P_o (0.22) that was only 48% that of P_o for a lone IP_3R (0.44) recorded under the same conditions (not shown). We conclude that the communication between IP_3R that allows clustering to reduce P_o must be mediated by physical contact between IP_3R, from which we can estimate the likely separations of lone and clustered IP_3R.

Our recordings from excised nuclear patches (estimated patch-pipette diameter ~1 μm) include a membrane area of at least 0.79 μm^2 (it may be larger if membrane is drawn into the pipette). The pores of neighbouring IP_3R (1.34 ± 0.13 IP_3R/patch; 1 IP_3R/0.59 μm^2) are therefore separated by an average distance of ~0.9 μm (i.e. the diameter of a patch with an area of 0.59 μm^2). After clustering, we suggest that neighbouring IP_3R must be in contact: their pores must therefore be ~18 nm apart (the diameter of an IP_3R)[42]. With an average of 4.25 ± 0.38 IP_3R/cluster (Figs 3c, g), and assuming that clusters (like lone IP_3R) are randomly distributed, each cluster must be accommodated in an area of membrane equal to 4.25-times that occupied by a single IP_3R (i.e. 2.51 μm^2, diameter = 1.8 μm). Hence the average separation of IP_3R clusters must be ~1.8 μm.

Time course of IP_3R3 diffusion and clustering

Our analysis of IP_3R clustering suggests that it proceeds with a half-time of about 1.5-2 s (k = ~0.4 s^{-1}) (Fig. 3i) and without need of the cytoskeleton (Supplementary Fig. 4). Two studies of IP_3R3 diffusion within ER membranes using fluorescence recovery after photobleaching (FRAP) suggest that most IP_3R3 are mobile[22] with a diffusion coefficient (D) of 0.03-0.04 μm^2/s (Ref. 22) or 0.45 μm^2/s (Ref. 21). We use an intermediate value, D = 0.1 μm^2/s, for our calculation of IP_3R3 mobility. The reaction rate (k) of proteins diffusing in a membrane patch can be estimated by Eq. 47 in Ref. 43:

$$k = N2\pi D/A\log(r^P/r^C) \qquad (\mathbf{9})$$

where,
N, number of channels per patch (2 in this example to give the lowest estimate of k).
D, diffusion coefficient (0.1 μm^2/s, see above).
A, area of patch (0.79 μm^2, see *Spacing of IP_3R before and after clustering*).
r^C, radius of IP_3R (9 nm, Ref. 42).
r^P, radius of patch (~0.5 μm).

from which, k = 0.91 s^{-1}.

These approximations suggest that diffusion alone (k = 0.91 s^{-1}) is sufficient to allow IP_3R3 to encounter each other with sufficient frequency to account for the estimated time course of IP_3R clustering (k ~0.4 s^{-1}, Fig. 3i, Supplementary Fig. 8).

Effects of IP_3R clustering on intracellular Ca^{2+} spiking

Our single channel analyses are best explained by the following gating scheme (Fig. 1d, Supplementary Fig. 6, Supplementary Table 1, and see *Analysis of patch-clamp records*):

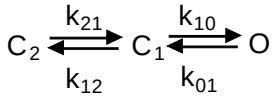

Channels move rapidly between C_1 and O (to give bursts of openings) and more slowly between C_2 and C_1 (to give long inter-burst intervals). Clustering of IP_3R has no effect on k_{10} (because the short-closed time, τ_c1, which is largely determined by k_{10}, is unaffected by clustering) or on k_{21} (because the long-closed time, τ_c2, is unaffected by clustering) (Supplementary Fig. 5, Supplementary Table 3). Clustering increases k_{01} (τ_o is shorter for clustered IP_3R, Fig. 3f) and this is alone sufficient to account for the observed decrease in P_o (Supplementary Fig. 6, Supplementary Table 4). The increase in k_{01} (from 84 s^{-1} to 185 s^{-1}) means that transitions from O to C_1 occur twice as frequently for clustered IP_3R. With no change in k_{10} or k_{12}, the more frequent visits to C_1 mean that the 'decision' on whether to move to C_2 (and so terminate a burst) or back to O (to give another short opening) is unchanged for clustered IP_3R but made twice as often as for lone IP_3R. The average number of openings in each burst is therefore the same for lone and clustered IP_3R, but the duration of the bursts is reduced for clustered IP_3R (Supplementary Table 4). The key point for our simulations is that shortening of τ_o (Fig. 3f) causes equivalent shortening of the bursts and entirely accounts for the changed behaviour of clustered IP_3R.

We simulate the cytosolic [Ca^{2+}] in a spherical cell (see Parameters Table 1) and examine the effect of IP_3R clustering on Ca^{2+} spikes. We give particular attention to the effects of changes in τ_o on the frequency of these Ca^{2+} spikes because Ca^{2+} signals in many cells are frequency-coded as intracellular Ca^{2+} spikes[1,44-46]. For our simulations, Ca^{2+} release from the ER is via IP_3R that open and close randomly according to the channel state dynamics described below. Ca^{2+} diffuses in the cytosol, where it is both bound to buffers and actively pumped back into the ER by SR/ER Ca^{2+}-ATPases (SERCA). The nonlinear parts of the concentration dynamics in the bulk (Ca^{2+} binding to buffers and transport by SERCA) are linearized, which is an excellent approximation for a wide range of parameters[47,48], and the concentration dynamics are solved by three-component Green's functions (Skupin and Falcke, unpublished). The channel state dynamics use the DeYoung-Keizer model (DK model)[49], which has been extensively used to simulate IP_3-mediated Ca^{2+} signalling[24]. The model assumes that each IP_3R has four identical subunits, each with a binding site for IP_3 and two Ca^{2+}-binding sites. A subunit is active if it has IP_3 bound, Ca^{2+} bound to the stimulatory Ca^{2+}-binding site, and no Ca^{2+} bound to the inhibitory Ca^{2+}-binding site. In the DK model, a channel is open when at least three of its four subunits are in the active state; otherwise it is closed. The open state of the IP_3R in the DK model corresponds to a burst in our single channel records. For the DK model, the current averaged over a burst (I_{burst}) is given by:

$$I_{burst} = I_s\tau_o/(\tau_o+\tau_c1)$$

where, I_s is the single channel current (estimated to be 0.12 pA)[47].

To allow burst length to be changed in accord with the experimental observations (ie decreased by ~50% for clustered IP_3R) within the framework of the DK model, the Ca^{2+} dissociation (k_{Cadiss}) rate was adjusted. It depends on τ_o:

$$k_{Cadiss} = b_5\tau_c 1(\tau_o+\tau_c 1)^{-1} \text{ (see Parameter Table 2).}$$

If we instead adjust the dissociation rate of IP_3 to be τ_o-dependent, the τ_o-dependent effects shown in Supplementary Fig. 7 are even more pronounced (not shown). We consider two arrangements of 32 IP_3R, each with the same overall channel density, but corresponding to the situations before and after IP_3-evoked clustering. Lone IP_3R (red in Supplementary Fig. 7a) separated by 1.5 μm (see *Spacing of IP_3R before and after clustering*)[24,50], and tight clusters of four IP_3R (blue) separated by 2.48 μm. We initially used regular configurations (rather than the random distributions observed experimentally, Fig. 1f) to avoid artifacts arising from specific configurations that might arise randomly (Supplementary Fig. 7b-d). Similar results were obtained when we used random configurations of clusters with the same average cluster density (Supplementary Fig. 7e).

Parameter Table 1 | Parameter values for the concentration dynamics

R	10 μm	Cell radius
a	8 nm	Channel radius
D_{Ca}	220 $\mu m^2 s^{-1}$	Diffusion coefficient of cytosolic Ca^{2+}
D_E	70 $\mu m^2 s^{-1}$	Diffusion coefficient of lumenal Ca^{2+}
D_B	95 $\mu m^2 s^{-1}$	Diffusion coefficient of mobile buffer
$[Ca^{2+}]_0$	48 nM	Basal cytosolic Ca^{2+} concentration
$[IP_3]$	0.4 μM	IP_3 concentration
$[B]_T$	45 - 65 μM	Total mobile buffer concentration
k_B^+	600 $(\mu Ms)^{-1}$	On rate of the mobile buffer
k_B^-	100 s^{-1}	Dissociation rate of the mobile buffer
$[B_i]_T$	30 μM	Total immobile buffer concentration
k_{Bi}^+	600 $(\mu Ms)^{-1}$	On rate of the immobile buffer
k_{Bi}^-	100 s^{-1}	Dissociation rate of the immobile buffer
P_p	100 s^{-1}	Pump rate
σ_p	$4.3x10^6$ s^{-1}	Channel flux constant
σ_l	~0.01 s^{-1}	Leak flux constant implicit given by P_p and $[Ca^{2+}]_0$

Parameter Table 2 | Parameter values for the DK model

a_1	20 $(\mu Ms)^{-1}$	IP_3 binding with no inhibiting Ca^{2+} bound
b_1	20 s^{-1}	IP_3 dissociation with no inhibiting Ca^{2+} bound
a_2	0.001 $(\mu Ms)^{-1}$	Ca^{2+} binding to Ca^{2+}-inhibitory site with IP_3 bound
b_2	0.03 s^{-1}	Ca^{2+} dissociation from Ca^{2+}-inhibitory site with IP_3 bound
a_3	2.6 $(\mu Ms)^{-1}$	IP_3 binding with Ca^{2+} bound to Ca^{2+}-inhibitory site
b_3	20 s^{-1}	IP_3 dissociation with Ca^{2+} bound to Ca^{2+}-inhibitory site
a_4	0.025 $(\mu Ms)^{-1}$	Ca^{2+} binding to Ca^{2+}-inhibitory site with no IP_3 bound
b_4	0.1 s^{-1}	Ca^{2+} dissociation from Ca^{2+}-inhibitory site without IP_3
a_5	10 $(\mu Ms)^{-1}$	Ca^{2+} binding to Ca^{2+}-activating site
b_5	1.225 s^{-1}	Ca^{2+} dissociation from Ca^{2+}-activating site

Supplementary References

27. Sugawara, H., Kurosaki, M., Takata, M., & Kurosaki, T. Genetic evidence for involvement of type 1, type 2 and type 3 inositol 1,4,5-trisphosphate receptors in signal transduction through the B-cell antigen receptor. *EMBO J.* **16**, 3078-3088 (1997).
28. Tovey, S. C., Sun, Y., & Taylor, C. W. Rapid functional assays of intracellular Ca^{2+} channels. *Nature Protocols* **1**, 258-262 (2006).
29. Rapp, G. & Guth, K. A low cost, high intensity flash device for photolysis experiments. *Pflüg. Archiv.* **411**, 200-203 (1988).
30. Walker, J. W., Somlyo, A. V., Goldman, Y. E., Somlyo, A. P., & Trentham, D. R. Kinetics of smooth and skeletal muscle activation by laser pulse photolysis of caged inositol 1,4,5-trisphosphate. *Nature* **327**, 249-252 (1987).
31. Qin, F. Restoration of single-channel currents using the segmental k-means method based on hidden Markov modeling. *Biophys. J.* **86**, 1488-1501 (2004).
32. Ding, S. & Sachs, F. Evidence for non-independent gating of $P2X_2$ receptors expressed in *Xenopus* oocytes. *BMC Neurosci.* **3**, 17-28 (2002).
33. Ching, L. L., Williams, A. J., & Sitsapesan, R. AMP is a partial agonist at the sheep cardiac ryanodine receptor. *Br. J. Pharmacol.* **127**, 161-171 (1999).
34. Mogami, H., Kanzaki, M., Nobusawa, R., Zhang, Y. Q., Furukawa, M., & Kojima, I. Modulation of adenosine triphosphate-sensitive potassium channel and voltage-dependent calcium channel by activin A in HIT-T15 cells. *Endocrinol.* **136**, 2960-2966 (1995).
35. McManus, O. B., Blatz, A. L., & Magleby, K. L. Sampling, log binning, fitting, and plotting durations of open and shut intervals from single channels and the effects of noise. *Pflüg. Archiv.* **410**, 530-553 (1987).
36. Sigworth, F. J. & Sine, S. M. Data transformations for improved display and fitting of single-channel dwell time histograms. *Biophys. J.* **52**, 1047-1054 (1987).
37. Sunderman, E. R. & Zagotta, W. N. Mechanism of allosteric modulation of rod cyclic nucleotide-gated channels. *J. Gen. Physiol.* **113**, 601-620 (1999).

38. Colquhoun, D. & Sigworth, F. J., in *Single-Channel Recording*, edited by B. Sakmann & E. Neher, Plenum Press, New York, pp. 483-587 (1995).
39. Colquhoun, D. & Hawkes, A. G., in *Single-Channel Recording*, edited by B. Sakmann & E. Neher, Plenum Press, New York, pp. 397-482 (1995).
40. Anantharam, A., Tian, Y., & Palmer, L. G. Open probability of the epithelial sodium channel is regulated by intracellular sodium. *J. Physiol.* **574**, 333-347 (2006).
41. Palmer, L. G. & Frindt, G. Amiloride-sensitive Na channels from the apical membrane of the rat cortical collecting tubule. *Proc. Natl. Acad. Sci. USA* **83**, 2767-2770 (1986).
42. da Fonseca, P. C. A., Morris, S. A., Nerou, E. P., Taylor, C. W., & Morris, E. P. Domain organisation of the type 1 inositol 1,4,5-trisphosphate receptor as revealed by single-particle analysis. *Proc. Natl. Acad. Sci. USA* **100**, 3936-3941 (2003).
43. Straube, R. & Falcke, M. Reversible clustering under the influence of a periodically modulated binding rate. *Phys. Rev. E* **76**, 010402-1-010402-4 (2007).
44. Falcke, M. On the role of stochastic channel behavior in intracellular Ca^{2+} dynamics. *Biophys. J.* **84**, 42-56 (2003).
45. Li, W.-H., Llopis, J., Whitney, M., Zlokarnik, G., & Tsien, R. Y. Cell-permeant caged $InsP_3$ ester shows that Ca^{2+} spike frequency can optimize gene expression. *Nature* **392**, 936-941 (1998).
46. Dolmetsch, R. E., Lewis, R. S., Goodnow, C. C., & Healy, J. I. Differential activation of transcription factors induced by Ca^{2+} response amplitude and duration. *Nature* **386**, 855-858 (1997).
47. Bentele, K. & Falcke, M. Quasi-steady approximation for ion channel currents. *Biophys. J.* **93**, 2597-2608 (2007).
48. Smith, G. D., Dai, L., Miura, R. M., & Sherman, A. Asymptotic analysis of buffered calcium diffusion near a point source. *SIAM J. Appl. Math.* **16**, 1816-1838 (2001).
49. De Young, G. W. & Keizer, J. A single-pool inositol 1,4,5-trisphosphate-receptor-based model for agonist-stimulated oscillations in Ca^{2+} concentration *Proc. Natl. Acad. Sci. USA* **89**, 9895-9899 (1992).
50. Dargan, S. L., Schwaller, B., & Parker, I. Spatiotemporal patterning of IP_3-mediated Ca^{2+} signals in Xenopus oocytes by Ca^{2+}-binding proteins. *J. Physiol.* **556**, 447-461 (2004).
51. Kenyon, J. L. & Bauer, R. J. Amplitude histograms can identify positively but not negatively coupled channels. *J. Neurosci. Methods* **96**, 105-111 (2000).

Supplementary Table 1 | Distributions of IP_3R3 before and after IP_3 pre-treatment

	IP_3R/patch	
	Mean ± SEM (n)	**Variance**
Naive	1.06 ± 0.15 (63)	1.39
IP_3 pre-treatment	1.03 ± 0.21 (88)	3.84
IP_3 treatment followed by washout	1.02 ± 0.18 (40)	1.26

Numbers of IP_3R/patch are shown for naive nuclei, after pre-treatment with 10 μM IP_3 for ~2 min and the latter followed by washout of IP_3 (see Figs 3a-d). For naive nuclei and those allowed to recover, the mean and variance are similar, consistent with a Poisson distribution. These comparisons include only results collected in parallel for the three conditions, the sample size (63 *vs* 109) and mean (1.06 *vs* 1.34) for naive nuclei are therefore slightly different from those cited in the text, which include results from all naive nuclei. Although the distribution of IP_3R between patches changed dramatically after IP_3 pre-treatment (Fig. 3a, c, and reflected in the increased variance above), the number of IP_3R/patch averaged over all patches was unaffected by IP_3, confirming that IP_3 affected neither the area of the patch nor our ability to resolve IP_3R activity.

Supplementary Table 2 | Properties of IP_3R3 within single and multi-IP_3R3 patches

Number of IP_3R	EC_{50}	maximal P_o
1	1.38 ± 0.03 μM	0.44 ± 0.05
2	2.02 ± 0.20 μM	0.25 ± 0.03
3	2.47 ± 0.25 μM	0.26 ± 0.02
4	ND	0.24 ± 0.02
5	ND	0.26 ± 0.03

From excised nuclear patches fortuitously containing the indicated numbers of IP_3R, the maximal open probability for each IP_3R (P_o) and the concentration-dependent effect of NP_o (EC_{50}) were computed (n = 3-7; 2 for the 5-IP_3R patch). For each concentration-effect relationship, curves were fitted to a Hill equation using non-linear unweighted least-squares regression, with error bars for EC_{50} values calculated from the sample variance of the residuals (GraphPad Prism). ND, not determined because too few recordings included 4 or 5 IP_3R to allow analysis of concentration-effect relationships.

Supplementary Table 3 | Effects of IP_3R clustering on closed times distributions

Number of IP_3R	Intra-burst closed time		Inter-burst closed time	
	τ_c1 (ms)	contribution	τ_c2 (ms)	contribution
1	1.4 ± 0.09	86 ± 6%	120 ± 9	14 ± 1%
2	1.05 ± 0.05	82 ± 6%	108 ± 11	16 ± 5%
3	1.05 ± 0.11	82 ± 2%	121 ± 17	16 ± 2%

Closed time distributions were fitted using the method of maximum likelihood[44] to recordings from patches containing 2 or 3 IP_3R after idealization with SKM in QuB (Supplementary Fig. 5). Because clustered IP_3R gate independently (Fig. 2f, Supplementary Figs 1, 2c), the long inter-burst intervals measured in multi-IP_3R patches (τ_{ib}) can be used to infer the underlying inter-burst intervals for individual IP_3R (τ_c2): $\tau_c2 = N.\tau_{ib}$. These calculated values of τ_c2 are shown in the table. The short intra-burst closed events (τ_c1) are unlikely to be significantly affected by the presence of other IP_3R, and are shown as directly determined from recordings of patches with lone or multiple IP_3R. The results demonstrate that neither τ_c1 nor τ_c2 is affected by clustering of IP_3R.

Supplementary Table 4 | Burst analysis of lone and clustered IP_3R3

	lone		clustered	
	observed	simulated	observed	simulated
P_o	0.44 ± 0.05	0.44 ± 0.02	0.24 ± 0.01	0.23 ± 0.01
τ_o (ms)	11.9 ± 1.6	12.6 ± 0.2	5.40 ± 0.5	5.5 ± 0.11
τ_b (ms)	143 ± 18	131 ± 6	ND	55 ± 1.7
n_b	14.5 ± 3	9.2 ± 0.5	ND	9.1 ± 0.6

Using the gating scheme shown in Fig. 1d, the activity of lone and clustered IP_3R (differing only in k_{01}) were simulated (for 20 s, n = 5) using QuB[60] (Supplementary Fig. 6). The table shows the properties (means ± SEM) of individual IP_3R either alone or within a cluster derived from burst analysis using ClampFit with a critical time of 10 ms. In addition to P_o and τ_o, the burst duration (τ_b) and number of openings per burst (n_b) are shown. The results demonstrate that the gating scheme faithfully replicates the observed gating parameters for both lone and clustered IP_3R.

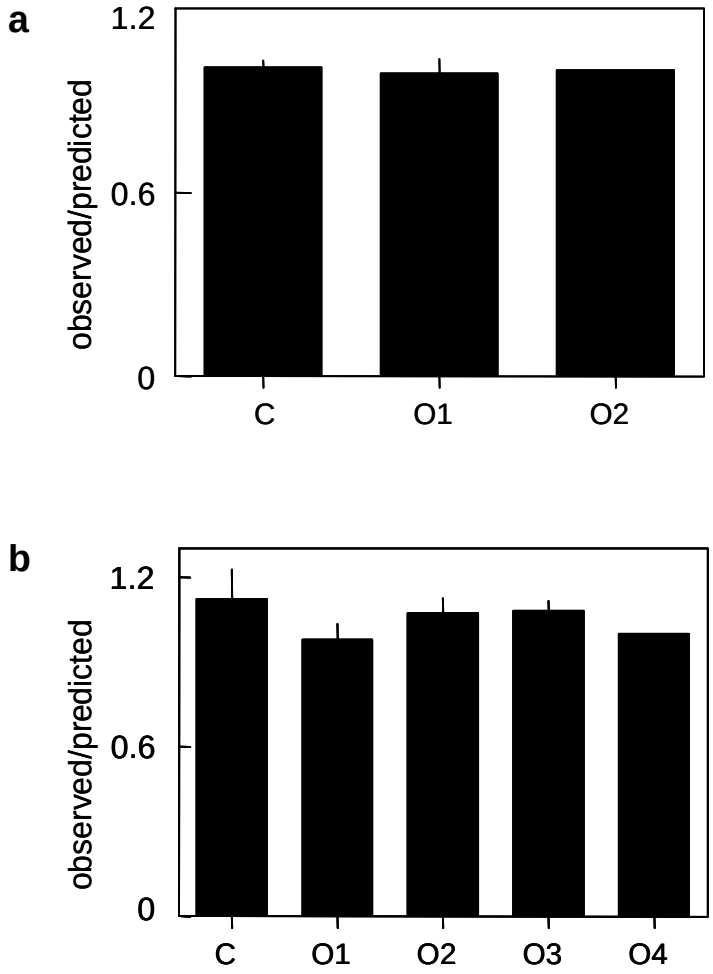

Supplementary Figure 1 | IP_3R3 open independently in patches containing multiple IP_3R3**. a**, **b**, For nuclear patches containing 2 (a) or 4 (b) IP_3R3, the binomial distribution was used to calculate probabilities for the indicated numbers of simultaneous openings for IP_3R stimulated with 10 μM IP_3 in 200 nM free Ca^{2+}. The histogram shows the observed probability divided by the predicted probability. These results, together with those in Fig. 2f, demonstrate that IP_3R open independently in patches with several IP_3R.

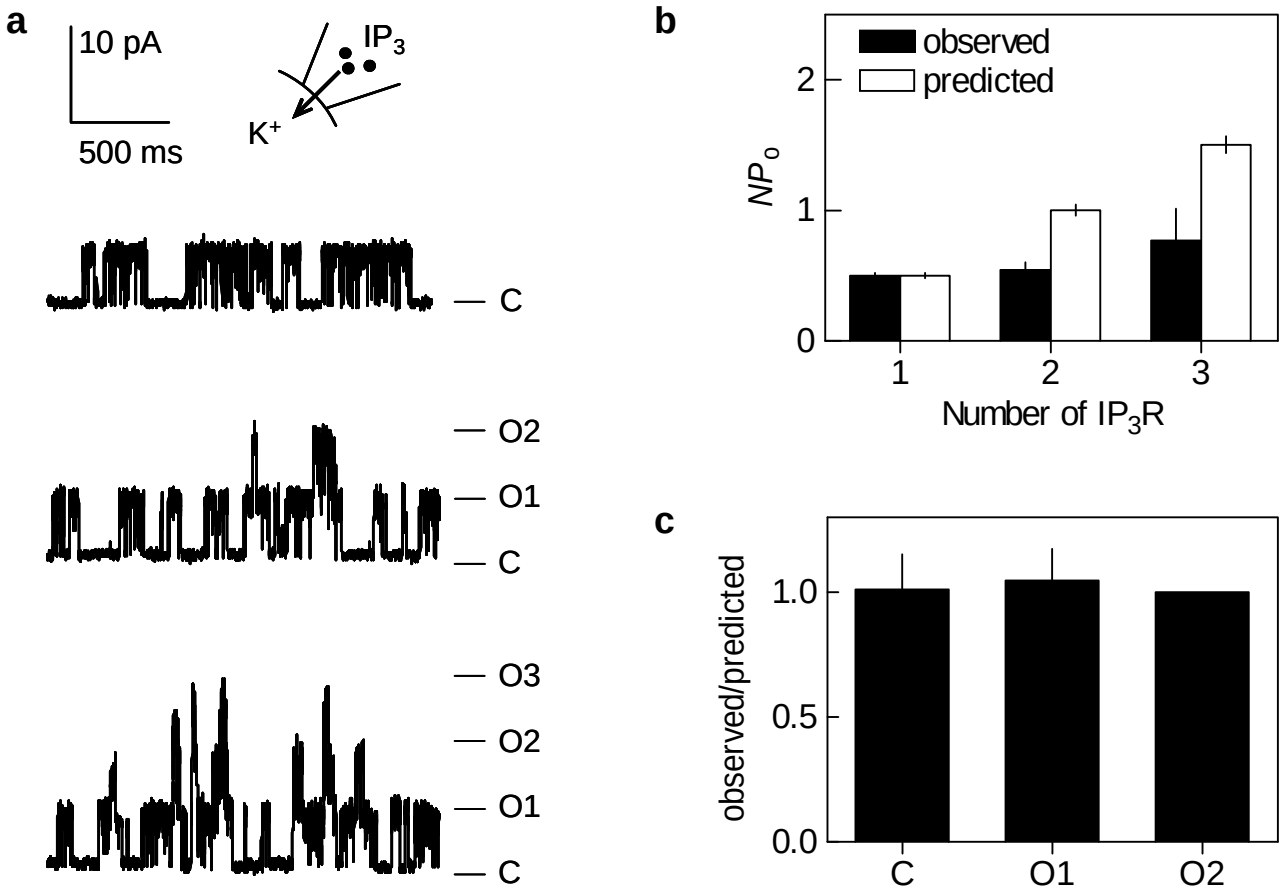

Supplementary Figure 2 | **IP_3-evoked clustering also inhibits IP_3R1**. **a**, Typical recordings from nuclei isolated from DT40-IP_3R1 cells at a holding potential of +40 mV and with 10 μM IP_3, 0.5 mM ATP and 200 nM free Ca^{2+} in PS. The recordings are from patches that included (top to bottom) 1, 2 or 3 IP_3R. C denotes the closed state. **b**, Observed and predicted NP_o for patches containing 1, 2 or 3 IP_3R ($n \geq 3$; n = 2 for the patch with 3 IP_3R). Predicted NP_o was calculated by assuming that P_o for each IP_3R within a multi-IP_3R patch has the same P_o as a lone IP_3R (ie P_{lone}). **c**, For patches containing 2 IP_3R, observed and predicted open probabilities are shown for the indicated open states. Predicted values were calculated from the binomial distribution (Supplementary equation 4). Observed/predicted values are shown (mean ± SEM, n = 5). These results establish that within patches containing more than one IP_3R1, each IP_3R opens independently, but to a lower P_o than for lone IP_3R1.

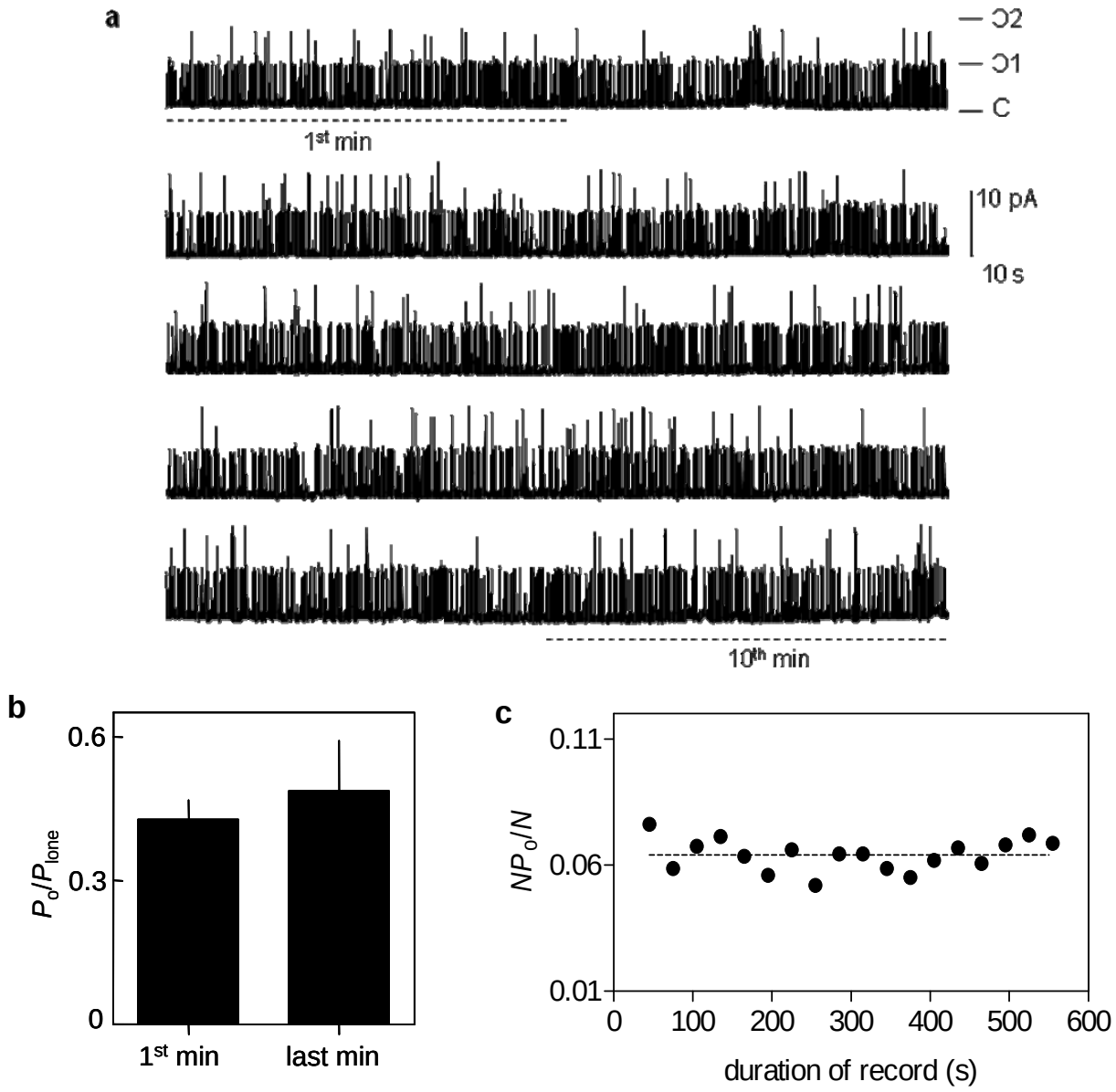

Supplementary Figure 3 | Sustained activity of IP_3R3 during sustained stimulation with IP_3. **a**, Typical 10-min recording from an excised patch containing 2 IP_3R stimulated with 1 μM IP_3 in PS containing 200 nM free Ca^{2+}. C and O denote closed and open states. **b**, From similar recordings, P_o was measured during the first and last minute of recordings that lasted 10-15 min from patches that contained 2 IP_3R. In all recordings, the estimated number of IP_3R was the same during each recording interval. P_o/P_{lone} was calculated from the binomial distribution (as in Fig. 3e); n = 4. **c**, Stability plot of the record shown in a. The results demonstrate that IP_3 causes IP_3R to attain their maximally inhibited state within the time taken to establish a recording (typically 30-45 s) and the activity remains stable thereafter for many min. We conclude that IP_3R clustering (reflected in P_o/P_{lone}) is complete within seconds of maximal stimulation with IP_3.

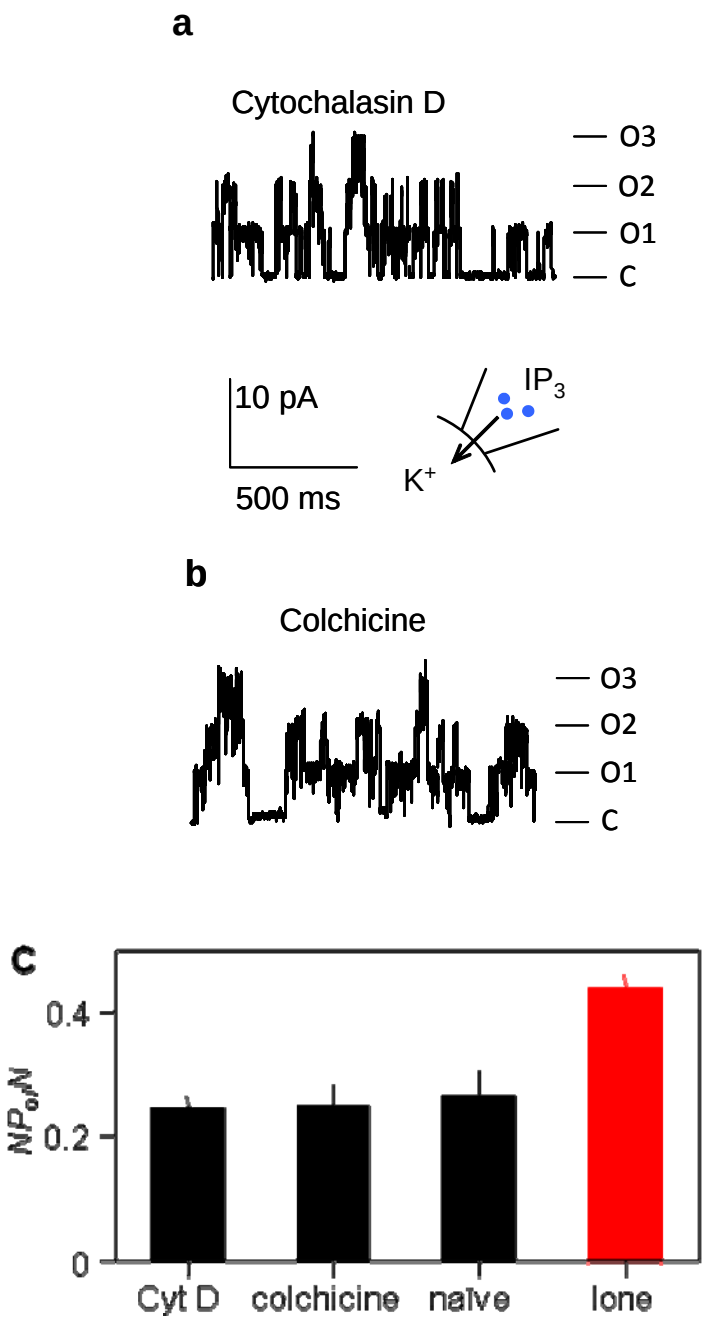

Supplementary Figure 4 | **IP_3-evoked clustering does not require the cytoskeleton**. **a**, **b**, Nuclei of DT40-IP_3R3 cells were pretreated with cytochalasin D (a, Cyt D, 20 µM, Calbiochem) to promote depolymerization of actin, or with colchicine (b, 100 µM, Sigma) to disrupt microtubules for 30 min before patch-clamp recording. Typical records from patches with three IP_3R are shown. C and O1-O3 denote the closed and open states. **c**, NP_o/N is shown for nuclear patches with 2-5 IP_3R (black) or for patches with a single IP_3R (red). Results are means ± SEM, n ≥ 3. The results demonstrate that disruption of the cytoskeleton does not affect IP_3-evoked clustering of IP_3R.

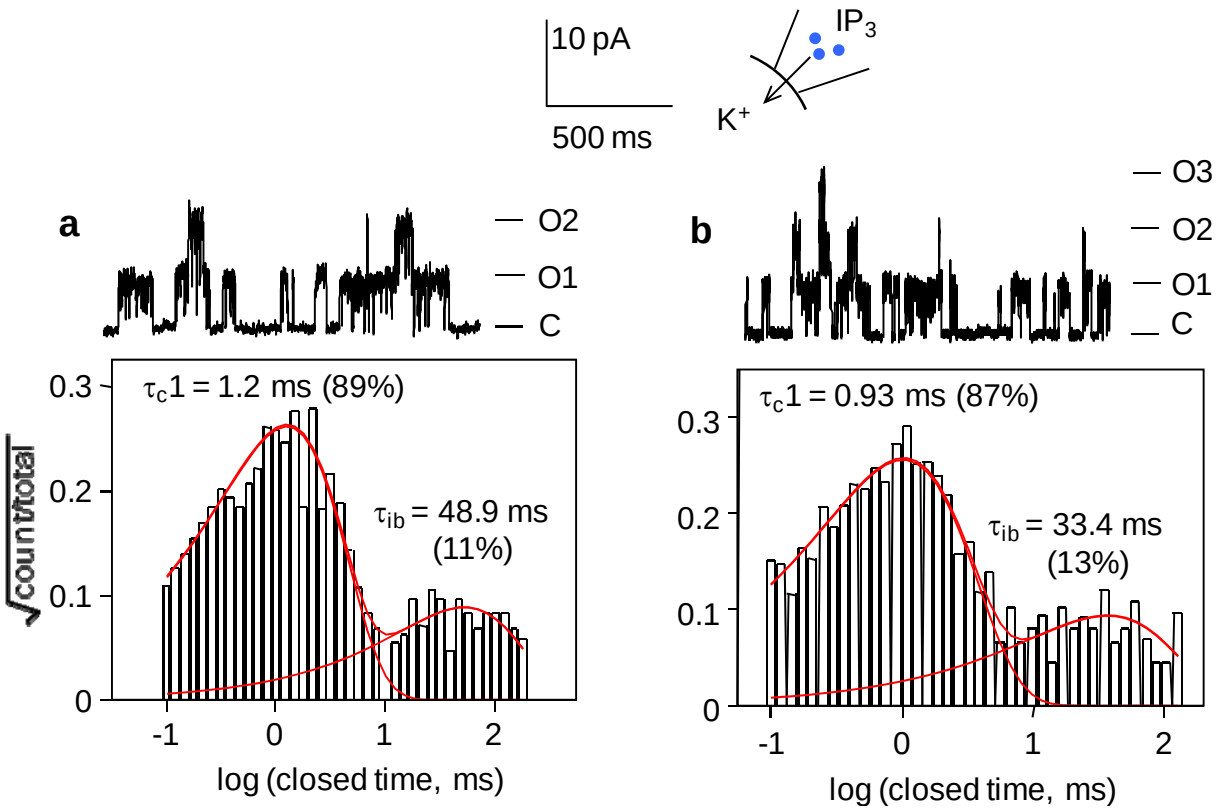

Supplementary Figure 5 | **Clustering has no effect on closed states of the IP$_3$R**. **a**, **b.** Typical recordings from patches with 2 (a) or 3 (b) IP$_3$R3, and their respective closed-time histograms. Empirical fitting of the closed time histograms identified two populations of closed states: τ_c1 representing closures within a burst and τ_{ib} representing closures between bursts. Because IP$_3$R open independently under these conditions (Fig. 2f, Supplementary Figs 1b, 2c), the inter-burst closed time for individual IP$_3$R within a cluster (τ_c2) can be calculated from: $\tau_c2 = N\tau_{ib}$ (Supplementary Table 3).

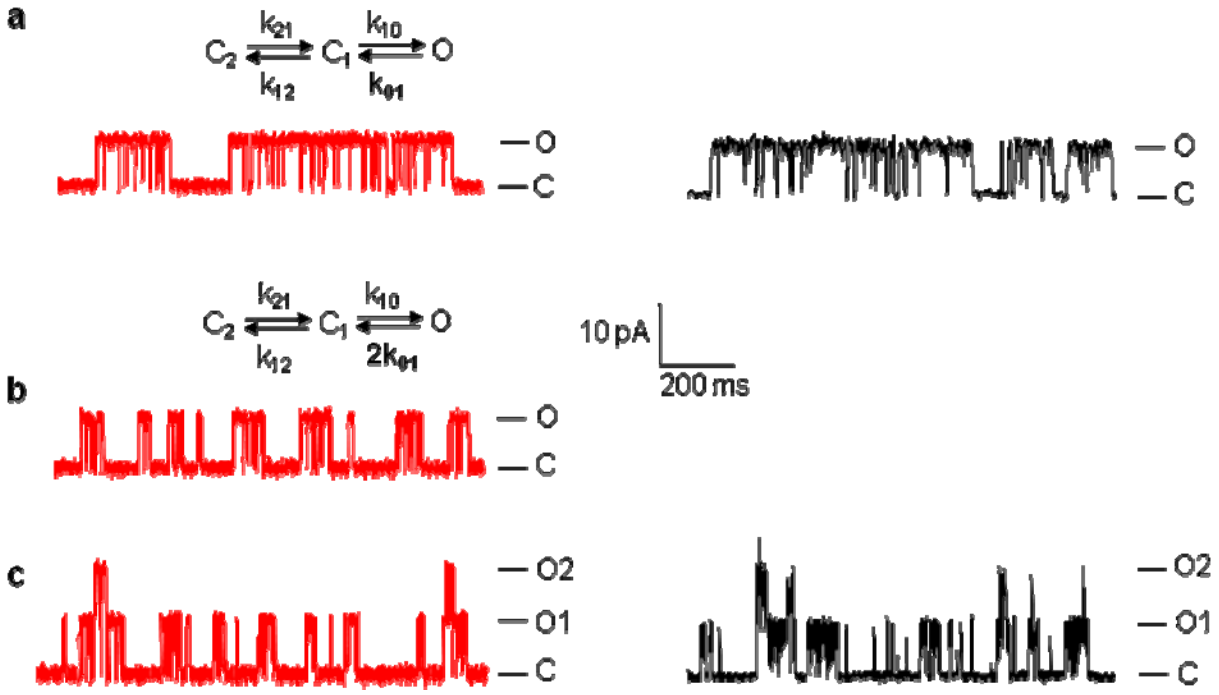

Supplementary Figure 6 | Comparison of observed and simulated activities of lone and clustered IP_3R. a, b, Typical observed (black) and simulated (red) IP_3R3 activities for lone IP_3R (a) or individual IP_3R within a cluster (b), each stimulated with 10 μM IP_3 and 200 nM free Ca^{2+}. The gating scheme is the same for each, but with k_{o1} doubled for clustered IP_3R. **c,** Behaviour of a cluster of 2 IP_3R. The noise (r.m.s noise) of real records was imposed during simulations and the records filtered at 1 kHz for display. C and O show closed and open current levels. Further details in Supplementary Table 4. The results show that the gating scheme faithfully captures the behaviour of lone and clustered IP_3R (Supplementary Table 4).

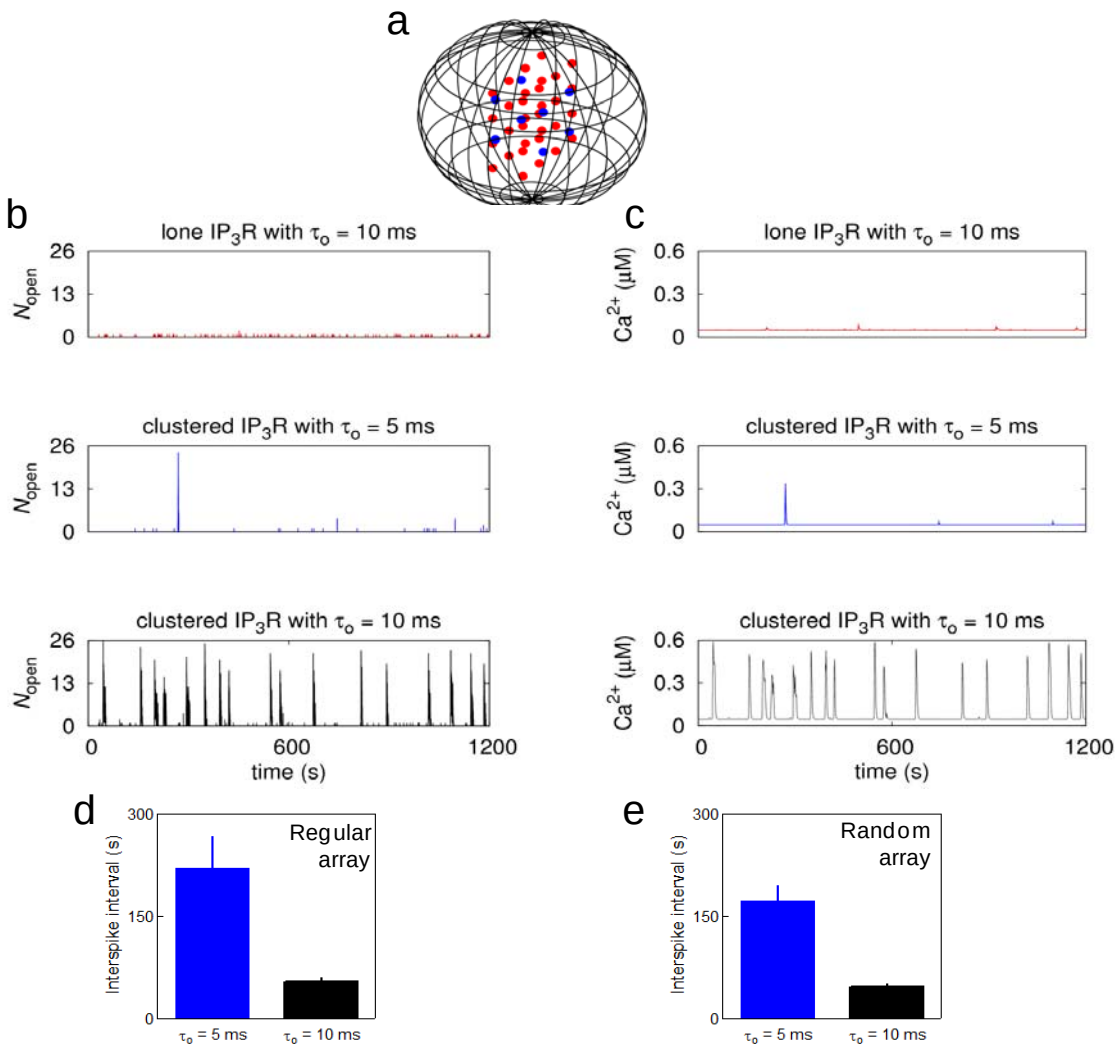

Supplementary Figure 7 | Clustering of IP_3R is required for Ca^{2+} spiking, and the decrease in τ_o caused by clustering profoundly affects the frequency of spiking. a, Simulations use either a regular array of 32 lone IP_3R (red) or a regular array of 8 clusters, each with 4 IP_3R (blue). The simulations compare the effects of decreasing τ_o from 10 ms to 5 ms, as described in Supplementary Discussion. **b**, **c**, Results of representative simulations show time courses for the numbers of open IP_3R (b) and global cytosolic free $[Ca^{2+}]$ (c). Comparison of the corresponding panels in b and c shows that the near simultaneous opening of several clusters is required to generate a Ca^{2+} spike. The behaviour of lone IP_3R is not sufficiently coordinated to generate a Ca^{2+} spike. **d**, Summary results from 10 independent simulations (means ± SEM) showing the mean interval between Ca^{2+} spikes, with each spike defined as an increase in free $[Ca^{2+}]$ of ≥ 0.25 μM. **e**, Similar analysis to d, but with randomly distributed clusters (n = 5 simulations). The mobile buffer concentration, $[B]_T$, was the same in all parallel comparisons of IP_3R behaviour. $[B]_T$ was 65 μM in b and c, 45-65 μM in d, and 60 μM in e. All other parameter values are given in Parameter Tables 1 and 2. The results demonstrate that for clustered IP_3R, a 2-fold decrease in τ_o causes the inter-spike interval (ISI) to increase by ~4-fold. The results confirm the importance of IP_3R clustering and the physiological significance of the decrease in τ_o associated with clustering.

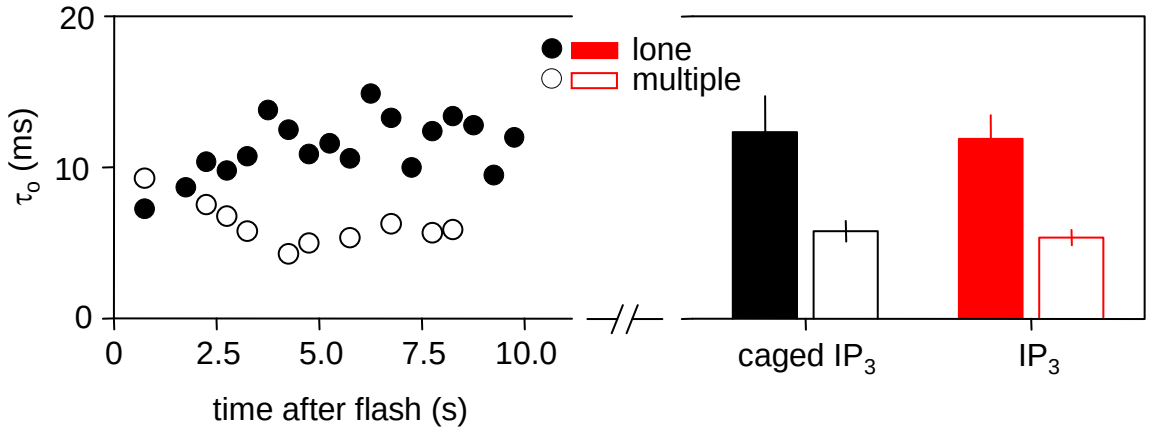

Supplementary Figure 8 | Kinetics of IP_3R3 clustering resolved by photolysis of caged IP_3. From experiments similar to that shown in Fig. 3h, τ_o was measured during each 0.5 s interval (1.5 s for the first interval) after photo-release of IP_3 within the patch-pipette. Results (means ± SEM for 4 patches with lone IP_3R, and 7 patches with 2-4 IP_3R) show that τ_o remains constant at 11.4 ± 0.5 ms for lone IP_3R, but rapidly falls to 5.8 ± 0.3 ms for IP_3R within multi-IP_3R patches. The histograms show the steady-state measurements of τ_o measured 5-120 s after flash-photolysis of caged IP_3 (black) and determined from experiments with IP_3 included in PS (red, as for Figs 1, 2). These results establish that after photo-release of IP_3, τ_o rapidly reaches a steady-state value identical to that determined by including IP_3 in the patch-pipette.

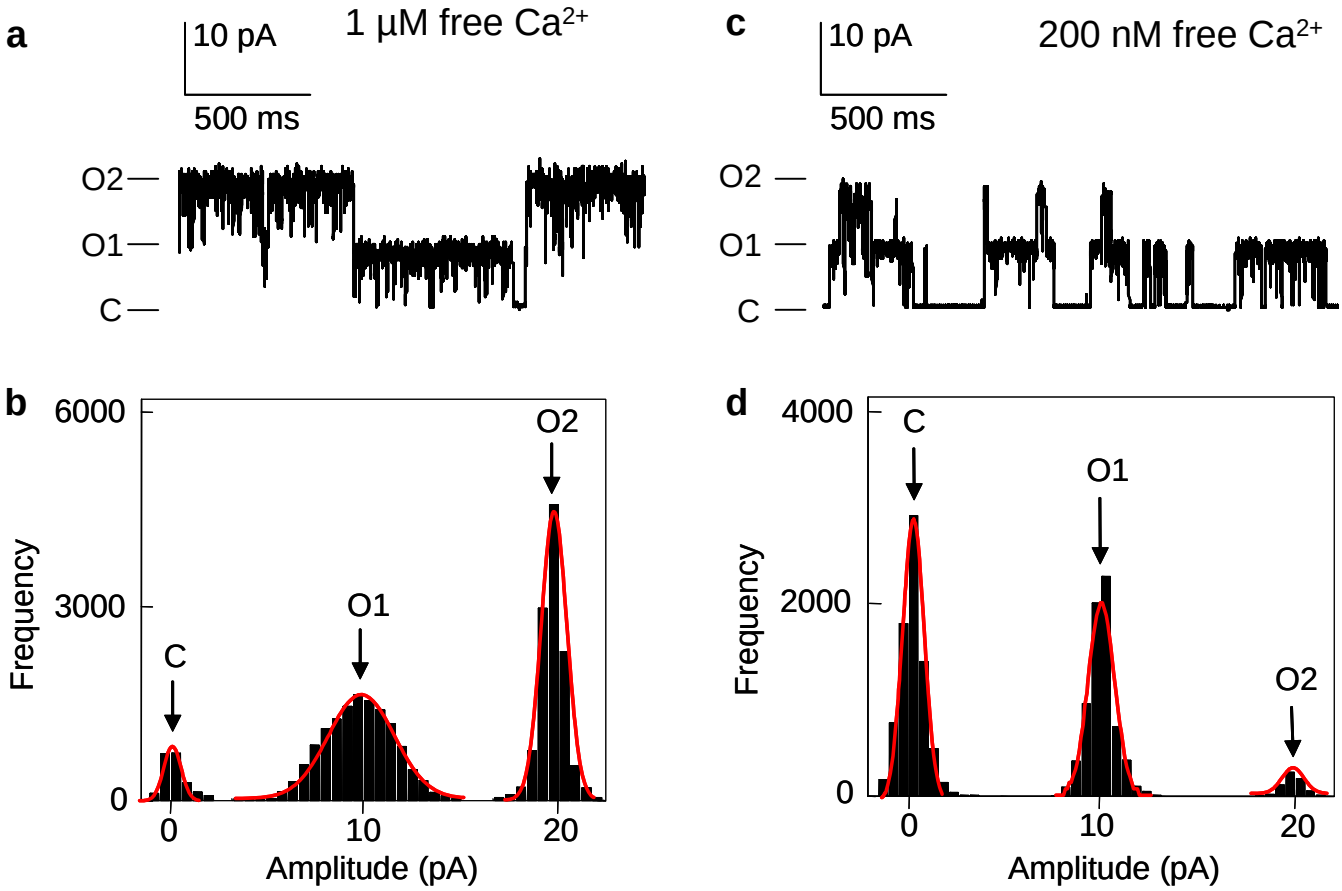

r
0.048
0.063
0.0811
0.0477
0.0841
0.1072

r	
-0.0033	0.0038
-0.0094	0.0000
	-0.0092
-0.0041	0.0007
-0.0024	0.0020
	-0.0022
-0.0044	
0.0005	

Supplementary Figure 9 | Coupled gating of clustered IP_3R stimulated with IP_3 and high Ca^{2+}. a, Typical recording from a patch with 2 IP_3R3 stimulated with 10 µM IP_3 and 1 µM Ca^{2+}. Closed (C) and the 2 open states (O1 and O2) are shown. **b**, Amplitude histogram of the recording shown in a, fitted (red line) to Gaussian distributions, from which the probabilities (P_c, $P_{o,1}$ and $P_{o,2}$) for each state (C, O1 and O2) were calculated. These values were used to calculate the "coupling factor", $r = -[(P_{o,1})^2/4] - P_c.P_{o,2}$; $r > 0$ denotes positively coupled gating of channels[51]. **c, d,** Show an equivalent trace and amplitude histogram for a patch with 2 IP_3R stimulated with 10 µM IP_3 and 200 nM Ca^{2+}. Values of *r* from 6 (1 µM Ca^{2+}) and 12 (200 nM Ca^{2+}) independent recordings are summarized below the appropriate panels. The results indicate that *r* is invariably > 0 for IP_3R stimulated at high Ca^{2+} (0.072 ± 0.009; consistent with positively cooperative gating), but generally ≤ 0 for IP_3R stimulated in 200 nM Ca^{2+} (-0.002 ± 0.001; consistent with a lack of positive co-operativity). This analysis further supports our conclusion (Fig. 4) that clustered IP_3R show coupled gating when Ca^{2+} is increased.